785 nm semiconductor laser with shallow etched gratings

Yue Yu-xin, Zou Yong-gang*, Fan Jie, Xiyao Fu, Zhang Nai-yu, Song Ying-min, Huang Zhuo-er, Ma Xiao-hui*

(*State Key Laboratory of High-Power Semiconductor Lasers, Changchun University of Science and Technology, Changchun 130022, China*)

**Corresponding author, E-mail: zouyg@cust.edu.cn , mxh@cust.edu.cn*

Abstract: A new type of 785nm semiconductor laser device has been proposed. The thin cladding and mode expansion layer structure incorporated into the epitaxy on the p-side significantly impacts the regulation of grating etching depth. Thinning of the P-side waveguide layer makes the light field bias to the N-side cladding layer. By coordinating the confinement effect of the cladding layer, the light confinement factor on the p-side is regulated. On the other hand, the introduction of a mode expansion layer facilitates the expansion of the mode profile on the P side cladding layer. Both these factors contribute positively to reducing the grating etching depth. Compared to the reported epitaxial structures of symmetric waveguides, the new structure significantly reduces the etching depth of the grating while ensuring adequate reflection intensity and maintaining resonance. Moreover, to improve the output performance of the device, a new epitaxial structure has been optimized. Based on the traditional epitaxial structure, an energy release layer and an electron blocking layer are added to improve the electronic recombination efficiency. This improved structure has an output performance comparable to that of a symmetric waveguide, despite being able to have a smaller gain area.

Key words: surface grating; etching depth; epitaxial structure; recombination efficiency; gain area

in press

具有浅刻蚀光栅的 785 nm 半导体激光器

岳钰新，邹永刚*，范杰，付曦瑶，张乃宇，宋英民，黄卓尔，马晓辉*

（长春理工大学大功率半导体激光器国家重点实验室，中国长春 130022）

摘要：我们提出了一种新型 785nm 半导体激光器件。在 P 侧外延中加入的薄限制层和模式扩展层结构，两者对光栅刻蚀深度的调节有很大影响。P 侧波导层的减薄使得光场偏向 N 侧包层。通过协调限制层的束缚效应，可以调节 P 侧的光限制因子。另一方面，模式扩展层的引入促进了 P 侧限制层上模式的扩展。这两个因素都有助于减少光栅蚀刻深度。与已报道的对称波导外延结构相比，新结构在确保足够反射强度和维持谐振的同时，大大减少了光栅的蚀刻深度。此外，为了提高器件的输出性能，还对新的外延结构进行了优化。在传统外延结构的基础上，增加了能量释放层和电子阻挡层，以提高电子复合效率。这种改进后的结构虽然增益面积较小，但输出性能却与对称波导相当。

关键词：表面光栅；蚀刻深度；外延结构；复合效率；增益面积

1 Introduction

Raman spectroscopy plays an important role in nondestructive testing. Portable, efficient, and convenient devices are preferred by consumers. Semiconductor lasers have garnered significant research attention due to their small size, light mass, and high electro-optical conversion efficiency, and can be used as Raman light sources when their excitation wavelength is 785 nm [1-2]. Raman detection requires high power (shortened detection time) and narrow linewidth (high spectral purity), which requires the product to have sufficient gain and the grating to have a high coupling coefficient κ, forcing the grating to have a high etching depth [3].

However, the ordinary wide-stripe laser has a wide gain spectrum, which makes multiple longitudinal modes to be excited and broadens the spectrum. As a wavelength selection element, the bragg grating filters the unwanted wavelengths and only retains the required Bragg wavelength. Such wider linewidths are not sufficient for Raman spectroscopy. Generally speaking, narrow linewidth lasers are categorized as external cavity lasers, distributed feedback lasers (DFB), and distributed bragg reflector lasers (DBR). External cavity lasers necessitate bragg gratings designed outside the cavity according to the diffraction conditions, which poses challenges in terms of mounting and light output efficiency. Consequently, intracavity design is the optimal choice. Regardless of whether it's DFB or DBR lasers, there's a need for sufficient etching depth to ensure an appropriate coupling coefficient. This presents numerous difficulties in laser fabrication, such as: shallow etching depth leading to inadequate mode filtering, large threshold current; Deep etching depth causing enhanced mode scattering and increased optical loss in the waveguide. In the meanwhile, excessively deep etching depth may also result in the formation of a V-groove, altering the effective duty cycle of grating and thereby affecting its coupling coefficient. To the author's knowledge, the vast majority of published papers related to epitaxial design usually keep the transverse mode profile as far away from the p-type region as possible, because the free carrier absorption coefficient of holes is higher than that of electrons (about three times higher). However, some articles do report that symmetric epitaxial structures yield higher reflectivity as well as optical confinement factors. Specially, the epitaxial structure adopted by the reported dual wavelength laser, taking Germany's FBH as an example, adopts a symmetrical waveguide and a 1 μ m wide cladding layer structure. This structure not only causes significant internal

in press

losses, but also requires deep etching to achieve the expected reflection effect [4-5]. The former issue presents challenges in the design of the transverse epitaxial structure: as the mode profile moves away from the p-side, the grating becomes weaker in coupling with the mode profile, leading to a lower coupling coefficient. To address this issue, we improve this situation by reasonably thinning the thickness of the P-side waveguide and introducing the mode expansion layer structure with certain internal losses. This strategy also yields additional benefits, for example, reducing the vertical divergence angle, raising catastrophic optical mirror damage (COMD) threshold, and boosting the output power and enhancing the refractive index difference to boost the coupling coefficient [6]. Near-infrared range (NIR) lasers suffer from low conversion efficiency due to the large bandgap energy of quantum wells, which results in easy electron leakage and reduces the internal quantum efficiency. To improve the injection efficiency of the electron and reduce the carrier escape phenomenon, this manuscript introduces an electron energy release layer in the n-side of the epitaxial layer. This layer enables high-energy electrons to recombine in the active region and release some of their energy in advance, increasing their likelihood of being captured by the quantum well. To mitigate the adverse effects of the escaped electrons, which usually accumulate and recombine on the p-side waveguide, causing the power drop, the concept of dual waveguide structure is proposed to counteract this issue. In addition, the lateral mode limitation is also an essential task. As the epitaxial layer structure changes, the width of the ridge varies with the change in the effective refractive index due to the mode cutoff condition. When designing the epitaxial structure, it is crucial to maintain an adequate lateral refractive index difference. Finally, the choice of the longitudinal mode is determined by the bragg grating, and it is known that there is a correlation between the grating order and the emission width (FWHM); that is, the lower the grating order, the broader the FWHM [7-8]. To ensure a sufficient coupling effect, we choose to use low-order DBR grating for mode-locking. To achieve sufficient output power, a long cavity length laser design is employed, which not only increases the optical amplification gain but also enhances heat dissipation. This results in a lower thermal resistance for the device.

Previous reports on the epitaxial structures of 785nm semiconductor lasers have predominantly employed symmetric waveguide (cladding) designs, necessitating deeper grating etching to achieve the desired reflectivity. This approach, however, frequently introduces heightened internal losses and poses numerous challenges during fabrication due to the larger etch

in press

depth-to-width ratio. Furthermore, excessively deep etching tends to create V-shaped grooves, which adversely impact the grating coupling coefficient. To address these issues, this manuscript proposes an innovative epitaxial structure that significantly reduces the grating etching depth while maintaining high-level output performance. The outline of this manuscript is as follows: The first part introduces the application value of 785 nm laser and the research method, the second part introduces the structure and design principle, the third part introduces the influence of different parameter conditions on the laser performance, and the fourth part summarizes the manuscript.

2 Device epitaxial structure design and theoretical analysis

The epitaxial layer structure is grown on a GaAs substrate through metal organic chemical vapor deposition (MOCVD). The thickness and doping concentration of each layer are elaborated in Section 3. Following epitaxial growth, the ridge waveguide of the distributed Bragg reflector (DBR) laser with a shallow etched grating structure is obtained by means of different lithography processes. The front and rear end surfaces are not coated after laser cleavage, resulting in an expected reflectivity of approximately 30%. The conventional laser structure consists of a substrate, buffer layer, upper and lower cladding layers, upper and lower waveguide layers, active region, and ohmic contact layer, which constitutes a simple structure with low beam quality. Building upon this foundation, a series of rational auxiliary layers are established to reduce resistance and loss and further enhance the output performance of the device. The details of these layers will be discussed in the subsequent section.

The maximum output power of a semiconductor laser is positively related to the COMD power density of the product with the following relationship [9]:

$$P_{\max} = \frac{d}{\Gamma_{QW}} W \frac{1-R}{1+R} P_{COMD} \tag{1}$$

where d is the quantum well thickness, Γ_{QW} is the active region confinement factor, R is the reflectivity of the front and rear cavity surfaces, and W is the device strip width. When the device quantum well width, front and rear cavity reflectivity, and device strip width are certain, the maximum output power of the device is inversely proportional to the optical confinement factor of the active region. The confinement factor is inversely correlated with the threshold current, and the maximum output power of the device is increased by appropriately lowering the confinement factor in the active region by reasonably setting the epitaxial structure.

The mode expansion layer is essential if we want to achieve a certain confinement factor to be maintained on the p-side. The

in press

confinement factor is expressed as the ratio of the light field intensity of a layer to the total light intensity and is defined by the equation:

$$\Gamma_i = \frac{\int_{y_{i-1}}^{y_i} H^2(y)dy}{\int_{-\infty}^{+\infty} H^2(y)dy} \quad (2)$$

where y_{i-1}, y_i represents the transverse position (the growth direction) of the layer, $H(y)$ is expressed as the distribution of the mode profile in the i_{th} layer. It can be known that the asymmetric waveguide is able to shift the mode profile to the n-side while the presence of the p-side extension layer keeps part of the mode profile on the p-side. However, the presence of too much mode profile can be a great waste of energy, and since the p-side holes have a stronger effect on light absorption, the relationship of internal losses has to be considered. The expression is [10]:

$$\alpha = \alpha_i + \alpha_m \quad (3)$$

$$\alpha_m = \frac{1}{2L} In \frac{1}{r_1 r_2} \quad (4)$$

$$\alpha_i = \frac{1}{p} \cdot \int \alpha(x)\left|E(x)\right|^2 dx \quad (5)$$

Where α, α_i, α_m are total optical loss, internal loss, and mirror loss, respectively. L is the cavity length, r is the reflectance of the front and rear cavity surfaces, $P = \int\left|E(x)^2\right|dx$, $E(x)$ is the distribution of the mode in the epitaxy direction. $\alpha(x) = \sigma_n n + \sigma_p p$, n and p are the densities of electrons and holes respectively, σ_n and σ_p are the absorption cross sections of the electrons and holes respectively.

Based on the above equations, it is evident that since the mirror reflectivity and cavity length are the same for each laser, the corresponding mirror losses are also equal. The distinguishing factor is that different epitaxial structures result in varying mode profile distributions within the devices, resulting in the mode profile overlapping with the waveguide and cladding layers to varying degrees, and then producing different internal losses. Among these, the p-side loss is particularly significant. Therefore, during the design of the mode expansion layer, considerations should be given to the p-side confinement factor and loss weighting analysis.

The simulation software employed for the simulation of semiconductor lasers is Crosslight from Canada - PICS3D [11]. This software enables the simulation of the energy band structure, gain profile, and output characteristics analysis of dedicated software for semiconductor lasers. The initial ridge width of the semiconductor laser is 5 μm, with a stripe width of 500 μm. The initial cavity length is assumed to be 1 mm and backg_loss to be 500 m^{-1}. The initial wavelength is 0.77 μm. Mirror_ref value of approximately 0.32.

in press

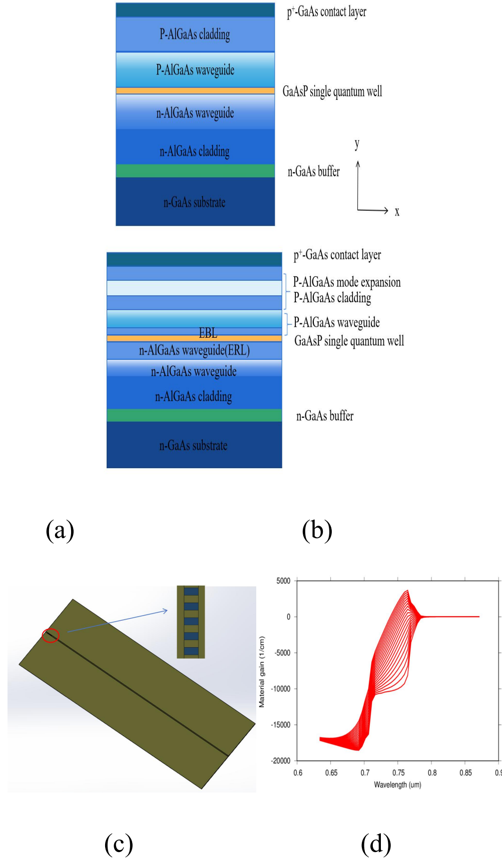

Fig.1. (a) Epitaxial structure of the traditional chip (b) epitaxial structure of the new chip (c)structure of the DBR laser (d) gain spectrum

3 Discussion and results

3.1 Epitaxial structure design

The growth material of the NIR laser typically consists of either GaAsP or AlGaAs system, the latter often contains Al component that is susceptible to oxidation, making the cavity surface susceptible to non-radiative recombination and burning. Nonetheless, AlGaAs exhibits higher electrical and thermal conductivity compared to GaAsP. Therefore, our research focuses on a GaAsP/AlGaAs system, where GaAsP serves as the well layer and AlGaAs forms the remaining layers for the 785nm epitaxial layer of the laser. It is widely recognized that increasing the number of wells can boost optical output power. However, an excessive number of wells can lead to different numbers of confined carriers among the wells, resulting in disparate gain. Furthermore, surpassing the critical limit for a number of quantum wells can cause stress release and generate numerous defects, significantly reducing the device's lifetime. The critical thickness can be expressed as:

$$h_c = \frac{a}{k\sqrt{2\pi f}} \frac{1-0.25\nu}{1+\nu}(1+In\frac{\sqrt{2}h_c}{\pi}) \quad (6)$$

Where h_c is the critical thickness, a is the lattice constant of the strain layer, $f = \frac{\Delta a}{a}$ is the mismatch degree, $\nu = \frac{C_{11}}{C_{11}+C_{12}}$ is poisson's ratio, k is a constant and takes the value of 4 for a single strain layer.

The lattice constant of GaAsP is smaller than that of GaAs substrate, leading to tensile stress in the active region, resulting in the dominance of the TM mode [12]. Taking into account the operation of the device due to thermal effects and the requirement to achieve a specific wavelength, the design of the epitaxial wafer should aim for a peak wavelength of a photoluminescence (PL) spectrum luminescence around 770 nm, with a single quantum well being accepted in the study. The reference and new epitaxial structure are shown in Fig. 1 (a) and (b), and the structure of the DBR laser as well as gain

in press

spectrum of this part structure is shown in Fig. 1 (d). The internal mode profile is mostly primarily transmitted along the waveguide layer, making the design of the waveguide layer essential. Enhancing the mode profile within the device can be achieved by employing various waveguide structures, such as symmetric waveguide, asymmetric waveguide, and extremely asymmetric structure (ETAS), which involve designing different epitaxial layers and optimizing composition [13-14]. Notably, the Al component has a linear relationship with the refractive index of $Al_xGa_{1-x}As$. Therefore, when designing the epitaxial wafer, it is crucial to ensure a gradual decrease in the refractive index from the active region towards both sides to limit the mode profile.

There is a relationship between the thickness of the waveguide layer D and the cutoff condition of the mode:

$$D = \frac{2\pi}{\lambda} t_w \sqrt{n_w^2 - n_{cl}^2} \tag{7}$$

where n_w, n_{cl} are the refractive index of the waveguide layer and the cladding layer, respectively, t_w is the total thickness of the waveguide layer and the cutoff condition of $D = m\pi$ the m-order mode.

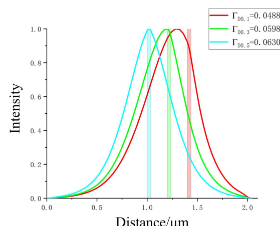

Fig.2 Mode field distribution for different p-side waveguide thicknesses

As can be seen in Fig.2, the shaded area indicates the overlap of the active region with the mode field. In the symmetric waveguide case, the active region overlaps with the optical field the most, making its confinement factor higher, and as the P-side waveguide is gradually thinned, the confinement factor of the active region decreases. The maximum output power of the asymmetric waveguide can be improved due to the lower optical confinement factor. The waveguide thickness and the divergence angle have the following relationship equation:

$$w_0 = t_c (0.31 + 2.2 / D^{3/2} + 30 / D^6) \tag{8}$$

$$\theta_{1/2} = 1.18 \tan^{-1}(\lambda / \pi w_0) \tag{9}$$

where w_0 is equivalent to a near-field Gaussian beam waist, $\theta_{\frac{1}{2}}$ is fast-axis divergence angle. The advantage of the asymmetric waveguide lies in the fact that the thinning of the p-waveguide not only biases the mode profile to the n-side, leading to lower internal optical loss but also reduces the series resistance.

The total thickness of the waveguide layer is determined by the cutoff condition, and after the thickness of the P-side waveguide is determined, which in turn determine the refractive index difference Δn between the waveguide and the cladding layer. As illustrated by Eq.7, it is known that when the

in press

refractive index of the waveguide layer is certain, a smaller difference of refractive index between the cladding and waveguide layers results in a larger critical thickness; when the refractive index of the cladding layer is certain, a smaller refractive index of the waveguide layer corresponds to a larger critical thickness. Smaller waveguide thickness, however, is insufficient to fully confine the mode profile within the waveguide layer, resulting in most optical modes leaking into the cladding layer; To facilitate fiber coupling in the subsequent stage, the vertical divergence angle should be reduced commonly. Therefore, the difference in aluminum component between the cladding layer and the waveguide layer should not be excessive in the selection of epitaxial materials.

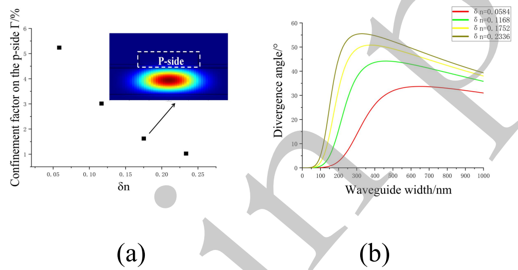

(a) (b)

Fig.3. (a) δn versus Γ (b) Waveguide refractive index, waveguide width versus divergence angle

Specially, we discuss the relationship between light confinement factor on the P-side and refractive index difference as well as the interrelation among different refractive index, different waveguide widths, and the divergence angle (FWHM). As depicted in Fig.3 shows the mode field distribution under asymmetric waveguide obtained by FDE. It can be clearly seen from the figure that most of the mode field is biased towards the N side of the device. And as the refractive index difference (δ n) between the waveguide layer and the confinement layer gradually increases, the optical field is more compressed in the waveguide layer, the optical confinement factor on the P side gradually weakens, the near-field becomes more concentrated, and the far-field divergence angle increases. If the difference is too small, it cannot form an optical waveguide to restrict the optical field. In order to reduce the etching depth of the grating, we need to keep the δn on the P side within a certain range. Meanwhile, it should be noted that if the thickness of the cladding layer is too thick, it will seriously affect the resistance of the device, and if it is too thin, it will lead to leakage of optical modes. Finally, we determine that the thickness of the cladding layer is chosen to be 400nm, and a suitable δ n of 0.175.

The total thickness of the waveguide layer is chosen to be within the range of the second-order mode cutoff rather than the first-order mode based on the fact that a reasonable widening of the waveguide layer thickness effectively mitigates the overlap of the mode profile with the cladding layer and prevents excessive losses. Despite the fact that a thicker the waveguide layer, the easier it is to produce higher-order modes, the confinement

in press

factor of the fundamental mode is much greater than that of the other modes, thereby placing it in a favorable position in the mode competition. Beyond that, increasing the total thickness of the waveguide layer within a specific range can reduce the fast-axis divergence angle. Considering the total waveguide thickness of 1000 nm within the second-order mode cutoff width.

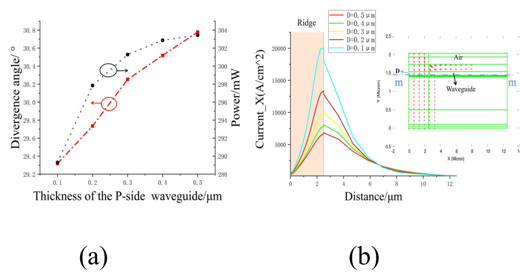

(a) (b)

Fig.4. (a) The relationship among different waveguide thicknesses and divergence angle and output power (b) Comparison of current density in the horizontal direction at different etching depths

Subsequently, it is crucial to settle on the thickness of the P-side waveguide (described in D). As illustrated in Fig.4 (a), on the premise that the total waveguide thickness remains unchanged, an increase in the thickness of P-side waveguide leads to an elevation in the output power and divergence angle [15]. Fig.4 (b) displays the current density at the interface (m-m cross section) between the upper barrier layer and the waveguide layer provided that the width of the ridge remains constant. On the one hand, the thinner P-side waveguide (thickness expressed as D) results in lower divergence angle, less internal loss, and reduced series resistance, leading to produce slight Joule heat. On the other hand, the confinement effect of the ridge waveguide curbs the lateral diffusion of carriers (X-direction), thus enriching the current in the ridge waveguide region. A thinner P-waveguide corresponds to a smaller effective gain area for the same cavity length, resulting in a lower output power. Ultimately, a p-waveguide thickness of 100nm is recommended to achieve a lower divergence angle.

To effectively enhance the output performance of the device, the gradient waveguide is employed to effectively reduce the voltage drop at the heterojunction interface, preventing the voltage loss generated by the abrupt heterojunction. Additionally, it inhibits the diffusion of some Al components into the active region.

Regrettably, there are still a few electrons escaping from the quantum well to the p-waveguide layer during the operation of the device, diminishing the efficiency of carrier recombination in the active region and generating parasitic recombination with the holes of the waveguide on the P-side. This results in a nonlinear output power, further restricting the application of the device [16]. Consequently, it is necessary to incorporate an inner waveguide as an electron barrier layer (EBL) between the last barrier and the waveguide, while maintaining the thickness of the p-side waveguide layer constant to

in press

mitigate the aforementioned damage. Simultaneously, as an EBL, it forms a stepped potential barrier in conjunction with the barrier layer. The following comparison examines the output power of lasers with internal waveguide structures of varying aluminum components.

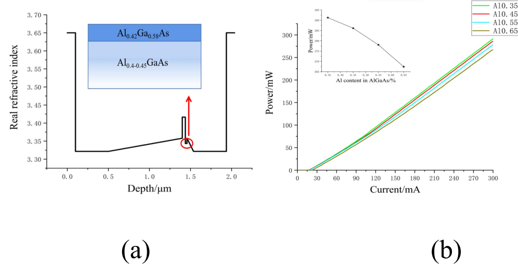

(a) (b)

Fig.5. (a) Refractive index of electron-blocking layer (b) output power at different components on the EBL

As illustrated in Fig.5 that the additional EBL fails to achieve the purpose of increasing power. Instead, the slope efficiency as well as output power decline as the aluminum component is incrementally (Al:0.35-0.65) increased under a 300mA working current. According to the formula:

$$\frac{1}{SE} = \frac{q\lambda}{hc\eta_{inj}}(1+\alpha_i \frac{1}{\alpha_m}) \tag{10}$$

where SE is the slope efficiency, q is the electron charge, λ is the excitation wavelength, h is the Planck constant, c is the speed of light, and η_{inj} is the injection efficiency. Based on the above equation, it can be seen that the slope efficiency is primarily associated to η_{inj}, α_i, α_m, because the reflectivity of the front and rear cavity surfaces of LD are the same, so the mirror losses α_m are equal. Changes in slope efficiency are related to the internal absorption loss (α_i), and current injection efficiency (η_{inj}). When the aluminum composition is around 0.45, the output power of the device is relatively objective, and the effect of EBL is more obvious. In order to better analyze the reasons for the decrease in output power, we calculate the optical field distribution and band structure when the aluminum composition is between 0.41-0.44, and the epitaxial structure without EBL is used as a reference group. Due to adjunction of the internal waveguide on the P side, compared to the structure without one, results in a reduction of the overall equivalent refractive index of the waveguide on the P side due to setting the layer composition, as well as a reduction in the refractive index difference with the cladding layer, so the light field is slightly shifted on the P side. However, the gradual increase of the aluminum component, the refractive index of the internal waveguide decreases, leading to an increase in the overall equivalent refractive index on the P side. This, in turn, increases the difference in refractive index between the waveguide and the cladding layer. As the refractive index difference increases, the mode profile shifts towards the N side shown in Fig.6 a), and the shift of the mode profile changes the active region confinement factor as well as the internal loss. However, Modification of the light field should lead to an increase in the slope

in press

efficiency of the device, thus the decrease in the device efficiency is due to the reduced injection efficiency of electrons.

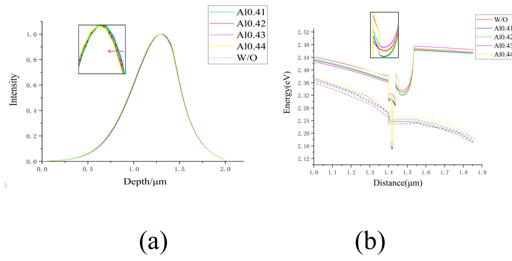

(a) (b)

Fig.6. (a) Light field distribution (b) Energy band diagram of different aluminum components

The injection efficiency of electrons is inversely correlated with the leakage of electrons due to the relationship between the magnitude of the leakage current and the bandgap of the p-side waveguide. A higher barrier makes it more challenging for electrons to transition to the p-waveguide. But contrary to this, the power decreases as the waveguide barrier increases. The energy band diagram shown above may provide a reasonable explanation for the above phenomenon.

From Fig.6 (b), it can be seen that an increase in the Al component of the p-side inner waveguide results in a decrease in the refractive index and an increase in the effective bandgap for electronic transitions within the p-side waveguide. With further increase in the bandgap, additional "pseudo wells" are created, leading to the recombination of carriers overflowing from the wells into the pseudo wells, as demonstrated by the enlarged image. The waste of carriers leads to a decrease in luminescence efficiency, which is also the reason why the output power does not increase but decreases instead [17]. In summary, it could be the case that the energy of injected electrons is excessive, coupled with internal loss and the presence of pseudo-wells, which prevent the electrons from being utilized effectively. Consequently, this leads to a decline in the luminescence efficiency.

To fundamentally enhance the recombination efficiency in the active region, it is necessary to confine the carriers supplied by the n-side cladding layer to the well as much as possible. Previous reports have focused on the structural design of the well or the barrier layer [18], which requires a robust confinement capacity of the well or higher bandgap of the barrier, making it difficult for the carriers to migrate outward. Another feasible option is to make the injected carrier energy lower, as reported in [19]. In this section, the effects of stepped waveguide, high refractive index constant waveguide, and low refractive index constant waveguide as the energy release layer (ERL) on the output performance, energy band structure, and electron carrier concentration distribution of the devices are discussed separately [20-21]. The electron composite efficiency is expressed as the ratio of the difference of electrons flowing into and out of a quantum well to the electrons flowing out at the last barrier layer. The total

in press

thickness of the N-side waveguide is 900nm for the following discussions.

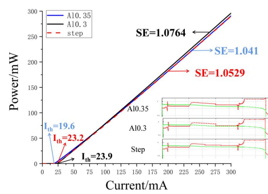

Fig.7. Comparison of output power of different structures

As seen in Fig.7: I): N-side inner waveguide with Al component of 0.35 and thickness of 0.4 μm; II): N-side inner waveguide component of 0.3 and thickness of 0.4 μm; III): stepped waveguide Al component of 0.35,0.37,0.4-0.45 and thickness of 0.3 μm are discussed respectively. As seen from the Fig.7, among them, the ERL structure with an aluminum composition of 0.35 exhibits a slope efficiency (SE) of 1.041 W/A, which is 3.39 % lower than that of the ERL structure with an aluminum composition of 0.3 (1.0764 W/A), and 1.13% lower than that of the stepped ERL structure (1.0529 W/A). the device corresponding to the high Al component has lower maximum power and lower threshold current, which is due to the lower energy of the waveguide layer, the electrons provided by the cladding layer release some energy in the waveguide layer, so that most of the electrons can be recombined in the well, accompanied by the EBL on the P side, and more carriers are recombined to generate photons, thus improving the efficiency. The bandgap of the high refractive index waveguide is narrower compared to the barrier layer, and the electrons also need to cross the barrier layer to participate in the recombination, reducing the recombination efficiency. However, at higher current, more electrons are recombined in the well, which elevates the output power. Step waveguide takes last place.

Previously, it was speculated that due to the high energy of the injected electrons, many electrons reside in the pseudo well, resulting in a reduced efficiency. This part is believed to play a role of electron absorption rather than electron blocking. To verify the speculation, the comparison of the output power and electron concentration distributions for the N-side with a ERL and the P-side with and without the EBL are conducted.

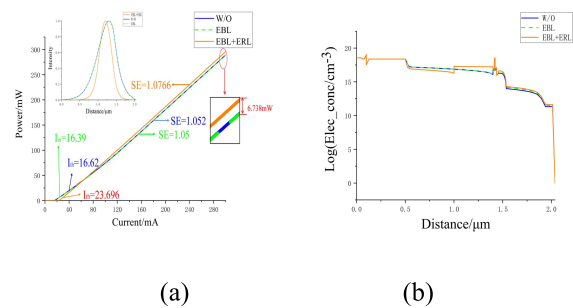

(a) (b)

Fig.8. (a) Comparison of output power and (b) electron concentration of different waveguide structures

It can be seen from Fig.8 that the chip incorporating EBL and ERL structures achieved an output power of 296.043mW and SE of 1.7066 W/A at an injection current of 300 mA. In comparison to a chip without these auxiliary layers, the output power and SE were enhanced by 2.32% and 2.34%, respectively.

in press

To further widen this performance gap, a strategy of moderately increasing the cavity length could be implemented. There is a difference in power with or without the EBL, while the EBL-only structure exhibits a lower threshold current, the output power is also low at high current. The inset figure displaying only the EBL reveals that the mode profile is biased towards the P-side, leading to higher losses and a seemingly higher threshold current, but the actual outcome is that the high-energy injected carriers flow back into the quantum well at low currents due to the EBL, but the output optical power at high injection current is generally lower than that with an ERL, due to the excess electrons not participating in the recombining in the well. In contrast, the epitaxial layers with EBL and ERL structures have a higher threshold current because of the lower light confinement factor in the active region. The Fig.8b) shows that under high current conditions, with an ERL on the N-side, more electrons will gather here to wait for the recombining in the well; while in the absence of an ERL, the concentration of injected electrons is lower, while the leaked electrons are essentially the same, so the structure with an ERL demonstrates a higher recombination efficiency and better performance. Although the EBL presents some obstacles, it does not entirely block the recombination of electrons on the p-side, which will be more significant in high current situations.

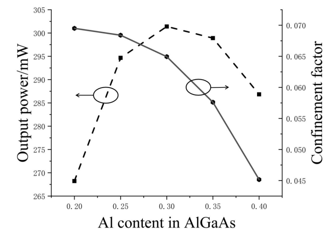

Fig.9. Effect of different Al components of ERL on output power and light confinement factor

In an effort to achieve increased output power, simulations are conducted on ERLs with varying components and thicknesses. From Fig.9, a higher light confinement factor in the active region and output power are observed when the Al composition is 0.3. When the thickness of the ERL is 0.1 μm, the output power reaches a high level which is not shown in this manuscript. Therefore, the component and thickness are 0.3 and 0.1 μm, respectively.

The mode extension layer is situated on the p-side, although it can cause a certain degree of optical loss. Nonetheless, the primary objective of this article is to reduce the etching depth of the grating. On the one hand, the extension layer needs to maintain a certain optical confinement factor on the p-side, allowing for shallow grating etching. On the other hand, it should not introduce excessive internal loss, which could exacerbate performance degradation. Furthermore， the refractive index of the extension layer needs to be higher than that of the cladding layer.

in press

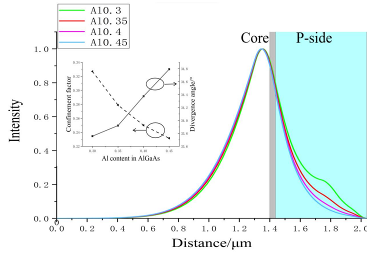

Fig.10. Simulated mode distribution for different Al contents. Inset shows their optical confinement factor on P-side and divergence angle

The following simulations are made separately: the thickness of the mode expansion layer is 0.1 μm and the distance from the waveguide layer is 0.2 μm. The effects of the size of different aluminum components of the mode expansion layer on mode distribution, the fundamental mode confinement factor on the P-side, and the divergence angle in fast axis are discussed. In addition, the grey area represents the location of the active area. It is seen from Fig.10 that as the refractive index of the mode extension layer increases (in the direction of component reduction), the confinement factors on the p-side increase, while the internal loss increases dramatically. The grey area denotes the location of the active area. When the aluminum component of the extended layer is approximately 0.35, among divergence angle, the internal loss and the P-side confinement factor remain moderate. Therefore, the choice of the component of the extended layer is 0.35. Furthermore, the effect of the distance between the mode expansion layer and the waveguide layer, as well as the thickness of the mode expansion on these characteristics are discussed again. Ultimately, the thickness of the mode expansion layer and distance between the mode expansion and waveguide layer are determined to be 0.1 μm.

Table 1 Parameter of each layer

Number	Layer	Material	Thickness/μm	Doping/m^{-3}
1	Top-cladding	$Al_{0.45}Ga_{0.55}As$	0.2	1e25
2	Mode expansion	$Al_{0.35}Ga_{0.65}As$	0.1	1e25
3	Lower-cladding	$Al_{0.45}Ga_{0.55}As$	0.1	1e25
4	waveguide	$Al_{0.45-0.4}GaAs$	0.08	none
5	Waveguide (EBL)	$Al_{0.42}Ga_{0.58}As$	0.02	none
6	barrier	$Al_{0.32}Ga_{0.68}As$	0.015	none
7	well	$GaAs_{0.83}P_{0.17}$	0.007	none
8	barrier	$Al_{0.32}Ga_{0.68}As$	0.015	none
9	Waveguide (ERL)	$Al_{0.3}Ga_{0.7}As$	0.1	none
10	waveguide	$Al_{0.4-0.45}GaAs$	0.8	none

in press

11	cladding	$Al_{0.45}Ga_{0.55}As$	0.4	1e25

The doping concentration of the cladding layer also has a significant impact on the output performance of the laser.

$$\rho_i = 1/\sigma_i = 1/n_i q \mu_i \tag{11}$$

where n_i, μ_i is the concentration and the mobility of the electrons (holes), q is electron charge. From the above formula, it can be seen that the higher the doping concentration, the lower the series resistance. To ensure sufficient output performance of the device due to the influence of material properties, we choose a high doping concentration cladding layer. The parameters of the optimized asymmetric waveguide structure are summarized in Tab.1.

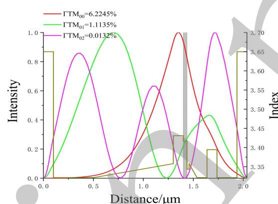

Fig.11. The refractive index and light field are distributed in the transverse direction

As shown in Fig.11, the gray area marks the position of the quantum well. And the fundamental mode has a greater overlap with the active region, while other higher-order modes have a lesser overlap with the active region. As a result, there are significant differences in the confinement factors among the three, which improves the gain difference and keeps the device in single transverse mode (fundamental mode) excitation, the remaining modes are suppressed in competition [22]. It is worth noting that the refractive index of the waveguide layer is higher than that of the active region, but its bandgap is still larger than that of the well's, thanks to the fact that the two belong to the different material systems, thus preventing the lasing (photoluminescence) wavelength from being changed.

It has been analyzed that the output power of traditional laser could reach 303.442mW with an injected current at 300mA due to its larger gain area. While the output power of optimized laser can be brought to the same level as that of the symmetrical and wide waveguide, which is 306.03 mW. However, compared with the asymmetric waveguide without an EBL and an ERL, the output power of new structure has been increased by approximately 20mW, thanks to its higher internal recombination efficiency. Therefore, the new structure exhibits lower internal losses and higher output power by rational optimization of the epitaxial structure.

3.2. Lateral Ridge Waveguide and Gratings Design

DBR lasers, being weak refractive index guided lasers, require lateral mode confinement to ensure the excitation of the fundamental lateral mode. A wider ridge width can lead to injected carriers producing sufficient gain for higher order modes, allowing them to participate in lasing and ultimately degrading the beam quality. The design of the ridge height also imposes stronger constraints on the mode profile.

$$W = \frac{\lambda}{2\sqrt{n_{eff}^2 - n_L^2}} \tag{12}$$

where W is the width of the ridge, λ is the wavelength, n_{eff} is the effective refractive index of the ridged waveguide part; n_L is the effective refractive index of both sides of the ridge waveguide; According to the above formula, the fundamental mode lasing can be realized when the ridge width reaches about 5 μm.

According to the coupling mode theory, the coupling coefficient is proportional on the reflectivity R. The length L of the grating has a great impact on the reflectivity, with the larger L is, the larger R is. But it's not necessarily true that a larger R is always better. It's been demonstrated that the coupling is best when $\kappa L \approx 1$. Where κL is referred to as coupling strength [23].

$$\Lambda = \frac{m\lambda_0}{2n_{eff}} \tag{13}$$

$$\kappa = \frac{2(n_m^2 - n_s^2)n_{eff}\sin(m\pi\gamma_{ac})}{m((1-\gamma_{ac})n_m^2 + \gamma_{ac}n_s^2)\lambda}\Gamma \tag{14}$$

$$R = \tanh^2(\kappa L) \tag{15}$$

where Λ is the period of the grating, m is the number of the order, n_{eff} is the effective refractive index, κ is the coupling coefficient. Γ is confinement factor. R is reflectivity, Δn is the refractive index difference between the etched zone and the unetched zone. From the above equation, it's evident that increasing the p-side confinement factor can lead to a higher coupling coefficient. Since the refractive index of the mode extension layer is higher than that of the cladding layer, the refractive index difference grows larger with increasing etch depth since the etch depth through the extension layer. We also need to consider the relationship between reflectivity intensity and the etching depth.

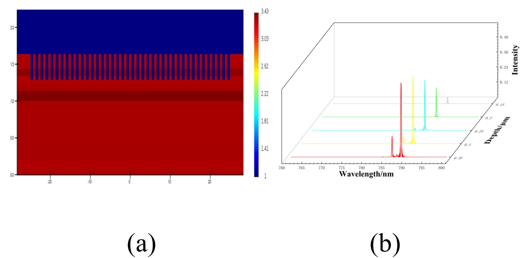

(a) (b)

Fig.12. a) Refractive index distribution of the grating b) The relationship between different etching depths and reflectivity

in press

The grating structure is simulated using the finite difference time domain method and its refractive index and reflectance distributions are shown in Fig. 12. The grating is designed to be etched on the P side of the epitaxial layer. The relationship between different etching depths and reflectance with mode extension layers are compared for the same number of grating pairs, period, and duty cycle. It can be seen that the reflection peaks of the device are gradually blue-shifted and increased as the etch depth increases. In addition, as the etched grating traverses the mode expansion layer (etching depth exceeding 0.2 μm), its reflectance is significantly enhanced. Due to the Full Width at Half Maximum (FWHM) of the reflection spectrum being less than 0.2 nm, the spectral line-width of the laser will be even narrower. To further narrow the line-width, increasing the order or the number of gratings can be effective strategies. When the depth of the grating of the symmetrically waveguide structure is 0.4μm, the optimized structure needs less than 0.3 μm depth to achieve the same reflectivity. In other words, the optimized device can be etched with shallower grating depths and still maintain resonance. The improved P-side epitaxial structure and grating etching depth are much smaller than the previously reported cladding layer thickness (1μm) and grating etching depth[1-2, 24].

4 Conclusion

In conclusion, the critical factor that affects the efficiency of the device is the electron injection efficiency. It is found that the design of the electron blocking layer on the p-side does not effectively improve the output power of the laser. The reason is that the introduction of the electron-blocking layer brings a pseudo-well where the high-energy injected electrons recombine, and for this reason, the energy of the electrons needs to be released in advance on the n-side, and it is observed that the injection efficiency can be improved by the combined effect of the constant waveguide and the electron blocking layer. Furthermore. The thinner epitaxial cladding and the mode expansion layer structure enormously reduce the grating etching depth. The laser with a mode extension layer has more prominent reflectivity in shallow etching conditions. The internal loss of the optimized structure is significantly reduced, and the output performance is improved to a certain extent compared with the symmetric waveguide structure.

Conflicts of Interest

The authors declare that there are no conf

in press

licts of interest relevant to this article.

Funding

This work was financially supported by the Jilin Science and Technology Development Plan (No. 20210201030GX), the Science and Technology Innovation Outstanding Team Project of Jilin Province (No. 20220508138RC). The Natural Science Foundation of Chongqing (Nos. CSTB2022NSCQ-MSX0889, CSTB2022NSCQ-MSX0401).

References

[1] Sumpf B, Kabitzke J, Fricke J, et al. Dual-wavelength diode laser with electrically adjustable wavelength distance at 785 nm[J]. Optics Letters, 2016, 41(16): 3694-3697.
[2] Sumpf B, Fricke J, Maiwald M, et al. Wavelength stabilized 785 nm DBR-ridge waveguide lasers with an output power of up to 215 mW[J]. Semiconductor Science and Technology, 2014, 29(4): 045025.
[3] Lei Y, Chen Y, Gao F, et al. 996 nm high-power single-longitudinal-mode tapered gain-coupled distributed feedback laser diodes[J]. Applied Optics, 2019, 58(23): 6426-6432.
[4] Tan S Y, Zhai T, Zhang R K, et al. Graded doping low internal loss 1060-nm InGaAs/AlGaAs quantum well semiconductor lasers[J]. Chinese Physics B, 2015, 24(6): 064211.
[5] Siyu E, Zhou Y L, Zhang X, et al. Simulation and experimental research of a high-order Bragg grating semiconductor laser[J]. Applied Optics, 2021, 60(21): 6076-6079.
[6] Al-Muhanna A, Alharbi A, Salhi A. Waveguide design optimization for long wavelength semiconductor lasers with low threshold current and small beam divergence[J]. Journal of Modern Physics, 2011, 2(04): 225.
[7] Holguín-Lerma J A, Ng T K, Ooi B S. Narrow-line InGaN/GaN green laser diode with high-order distributed-feedback surface grating[J]. Applied Physics Express, 2019, 12(4): 042007.
[8] Siyu E, Zhou Y, Zhang X, et al. High-order DBR semiconductor lasers: effect of grating parameters on grating performance[J]. Applied Optics, 2020, 59(28): 8789-8792.
[9] Abbasi S P, Goodarzi M, Mahdieh M H. Optimization of AlGaInAs quantum well in semiconductor lasers[J]. Optical and Quantum Electronics, 2022, 54(8): 517.
[10] Pikhtin N A, Slipchenko S O, Sokolova Z N, et al. Internal optical loss in semiconductor lasers[J]. Semiconductors, 2004, 38: 360-367.
[11] http://crosslight.com.cn
[12] Erbert G, Bugge F, Knauer A, et al. High-power tensile-strained GaAsP-AlGaAs quantum-well lasers emitting between 715 and 790 nm[J]. IEEE Journal of selected topics in quantum electronics, 1999, 5(3): 780-784.
[13] Kaul T, Erbert G, Maaßdorf A, et al. Extreme triple asymmetric (ETAS) epitaxial designs for increased efficiency at high powers in 9xx-nm diode lasers[C]//High-Power Diode Laser Technology XVI. SPIE, 2018, 10514: 53-59.
[14] Botez D. Design considerations and analytical approximations for high continuous-wave power, broad-waveguide diode lasers[J]. Applied Physics Letters, 1999, 74(21): 3102-3104.
[15] An N, Dong X, Song Q, et al. Optimization for designing the waveguide of 980 nm AlGaAs/InGaAs semiconductor laser[J]. Optik, 2015, 126(22): 3477-3481.
[16] Xu B, Qu K, Wang Z, et al. Investigation of photoelectric performance of laser diode by regulation of p-waveguide layer thickness[J]. Optik, 2020, 200: 163458.
[17] Zubov F I, Maximov M V, Shernyakov Y M, et al. Suppression of sublinearity of light–current curve in 850 nm quantum well laser with asymmetric barrier layers[J]. Electronics Letters, 2015, 51(14): 1106-1108.

in press

[18] Yang J, Zhao D G, Jiang D S, et al. Performance of InGaN based green laser diodes improved by using an asymmetric InGaN/InGaN multi-quantum well active region[J]. Optics Express, 2017, 25(9): 9595-9602.
[19] Yang J, Zhao D, Liu Z, et al. Suppression the leakage of optical field and carriers in GaN-based laser diodes by using InGaN barrier layers[J]. IEEE Photonics Journal, 2018, 10(4): 1-7.
[20] Li X, Zhao D, Jiang D, et al. Suppression of electron leakage in 808 nm laser diodes with asymmetric waveguide layer[J]. Journal of Semiconductors, 2016, 37(1): 014007.
[21] Yang J, Zhao D G, Zhu J J, et al. Effect of Mg doping concentration of electron blocking layer on the performance of GaN-based laser diodes[J]. Applied Physics B, 2019, 125: 1-5.
[22] Yang J, Zhao D G, Jiang D S, et al. Enhancing the performance of GaN based LDs by using low In content InGaN instead of GaN as lower waveguide layer[J]. Optics & Laser Technology, 2019, 111: 810-813.
[23] Yang J, Fan J, Zou Y, et al. Dual-wavelength operation of a tapered laser diode based on a composite DBR grating near 1.03 μm[J]. Optics Letters, 2022, 47(9): 2141-2144.
[24] Theurer, L. S., Sumpf, B., Maiwald, M., Fricke, J., Ginolas, A., & Tränkle, G. (2021). Ten emitter dual-wavelength Y-branch DBR laser diode array emitting 1 W at 785 nm with a spectral emission width below 60 pm. Journal of Physics Communications, 5(10), 105017.

Author Biographics：

Yuxin Yue is a Ph.D. candidate, currently pursuing his Ph.D. degree at the State Key Laboratory of High Power Semiconductor Laser, Changchun University of Science and Technology. His main research interests include device design and packaging of semiconductor lasers.

Yonggang Zou, born in 1982, male, researcher, Changchun University of Science and Technology. received his Ph.D. degree from Jilin University in 2009, majoring in condensed matter physics. He is mainly engaged in the research of optoelectronics technology and application.

Xiaohui Ma, professor, doctoral supervisor, is the director of the State Key Laboratory of High Power Semiconductor Laser at Changchun University of Science and Technology. He is the overall expert of “Strategic Advanced Electronic Materials” of National Key R&D Program, the chief scientist of “173” project of Military Science and Technology Commission, the director of Optical Engineering Society of China, the member of National Optoelectronic Measurement Standardized Technical Committee, and the Distinguished Professor of Changbaishan Scholars of Jilin Province. He is also a special professor of Changbaishan Scholars in Jilin Province. His main research direction is optoelectronic technology and application.

in press